Finite Element Method for Computing Turbulent Propeller Flow

Dominique Pelletier,* André Garon,† and Ricardo Camarero‡
Ecole Polytechnique de Montréal, Montreal, Quebec, Canada

A numerical procedure based on the primitive variable Navier-Stokes equations is applied to the simulation of the three-dimensional axisymmetric flow near a propeller in a uniform flow. The time-averaged Navier-Stokes equations are solved using both a mixed and a penalty function finite element method. A new model is developed to compute axisymmetric viscous throughflow past propellers. This is achieved by forcing the flow to be tangent to the mean stream surface between the blades. This condition is enforced by introducing a Lagrange multiplier that can be interpreted as the force applied by the blades on the fluid. Turbulence is modeled by a simple mixing length equation. Detailed comparison with wind tunnel measurements shows good prediction of velocity and pressure. The present approach represents a first step toward the development of a viscous quasi-three-dimensional capability.

Nomenclature

D	= propeller diameter
$D_t(\cdot)$	= material derivative operator
$\boldsymbol{D} \subset \Omega$	= propeller domain
$\boldsymbol{e}_x, \boldsymbol{e}_r, \boldsymbol{e}_\theta$	= cylindrical coordinates unit vectors
$\boldsymbol{F}$	= global right-hand side vector and blade force
f	= blade force, $= f_v + f_s \delta_s$
f_v	= volume force
f_s	= surface force
g	= metric tensor
K	= global system matrix
$\boldsymbol{n}$	= unit outward normal vector
p	= pressure
R_0	= propeller radius
S_1, S_2	= blade-to-blade and throughflow stream surfaces
$\boldsymbol{s}$	= stream surface normal vector
t_s	= surface traction, $= -p\boldsymbol{n} + \mu\tau \cdot \boldsymbol{n}$
$\bar{U}$	= global vector of unknowns
$\bar{U}_r$	= fluid velocity relative to the blade
$\boldsymbol{u}$	= velocity vector
u_i	= ith component of $\boldsymbol{u}$
u_x, u_r, u_θ	= cylindrical components of $\boldsymbol{u}$
$\boldsymbol{v}$	= propeller entrainment velocity vector, $= r\omega \boldsymbol{e}_\theta$
μ	= effective viscosity, $= \mu_l + \mu_t$
μ_l	= laminar viscosity
μ_t	= turbulent eddy viscosity
ρ	= density
σ	= stress tensor, $-pg + \mu\tau$
τ	= strain rate tensor, $= \text{grad}(\boldsymbol{u}) + \text{grad}(\boldsymbol{u})^T$
ω	= propeller angular velocity
Ω	= computational domain
∂D	= boundary of $\boldsymbol{D}$
$\partial\Omega$	= boundary of the computational domain

Presented as Paper 87-0048 at the AIAA 26th Aerospace Sciences Meeting, Reno, NV, Jan. 11–14, 1988; received April 12, 1989; revision received Nov. 29, 1989.

*Professor, Applied Mathematics Department. Also Adjunct Professor Aerospace Engineering, Virginia Polytechnic Institute and State University, Blacksburg, VA. Member AIAA.
†Research Fellow, Applied Mathematics Department.
‡Professor, Applied Mathematics Department.

Introduction

DETAILED analysis of the flow produced by components of rotating machinery such as propellers, windmills, rotor-stator combinations, turbines, pumps, and mixers, is required for the performance evaluation of such equipment. Examples include the prediction of the near-wake profiles of propellers and losses in turbines and pumps, to name a few. State-of-the-art techniques make it possible to compute turbulent flow in the various components of a turbomachine taken separately,[1] and some results are available for the simulation of multiblade row turbomachinery flows.[2,3]

Even with present day computers, the numerical treatment of the fully three-dimensional, unsteady flow around a set of individual blades with their thin boundary layers and wakes represents a task that is too great to be attempted at this time. Until recently, only approximate analytical treatments were available involving one or more of the following restrictive assumptions: the flow was assumed inviscid or laminar, the propeller was represented as an actuator disk with constant thrust, and the effects of the propeller on the flowfield were assumed small enough to permit linearization. References 4–6 are representative. Previous numerical work on propellers and windmills[7,8] required knowledge of the dynamics of the rotor. Thrust and torque were introduced via body forces distributed in the volume occupied by the rotor (this approach is akin to actuator disk theory[5,9]). The biggest limitation of such an analysis is the necessity to rely on experimental values of thrust and torque.[7]

This work is part of an ongoing effort towards removing this limitation while retaining most of the simplicity of previous computational approaches. Incorporation of the kinematics of the rotor into the Reynolds-averaged Navier-Stokes equations (i.e., specification of the mean stream surface in the bladed region) gives rise to an additional equation supplementing the equations of motion. This relationship expresses the work done by the propeller on the fluid. The present approach makes it possible to treat complex systems such as a complete pump, counterrotating propellers, or propulsors. A propulsor is a combination of a propeller producing the bulk of the thrust and a fixed set of blades designed to extract extra thrust from the kinetic energy of the swirl generated by the propeller.

Wu's method[10] has been used for over 30 years in solving inviscid cascade flows. The present approach is a rigorous two- and three-dimensional extension to viscous flows. By requiring the flow to be tangent to the mean throughflow (S_2 on Fig. 1) stream surface in the bladed region, the blade force arises naturally. Hence the need to prescribe thrust and

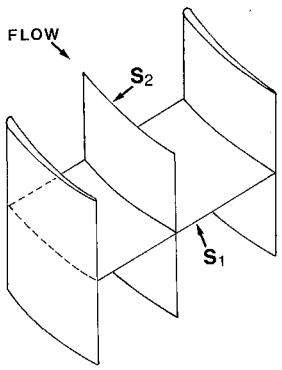

Fig. 1 Wu's stream surfaces.

torque from experiment is replaced by the specification of the shape of the mean stream surface. Such data are provided by blade-to-blade calculations in a quasi-three-dimensional analysis or by a simpler approximation, as in the present case. The method developed here results in a velocity, pressure, blade-force formulation of the fully elliptic time-averaged Navier-Stokes equations for an incompressible fluid. In the case of rotors, the analysis provides the thrust, torque, and power input to or extracted from the flow. The computational method is fast enough to be useful in a design environment.

The key element of our approach is the modeling of the effects of the blades on the flowfield. First, we describe a model of blade effects that leads to the augmented Navier-Stokes equations, the basis for our analysis. Two simple cases with analytical solutions provide insight into the behavior of the blade-force terms. The development of the model for a given propeller is then given. The finite element solution algorithm is then described. Details of the nonlinear equation solver are given. Numerical results for the experimental conditions of Ref. 11 complete this paper.

Modeling of the Problem

This section outlines the key features of our analysis: the blade effects and equations of motion and their use in simulating a given propeller.

New Model for Blade Effects

In Wu's original analysis,[10] the equations of motion for an inviscid compressible flow are written for two families of stream surfaces: blade-to-blade (S_1) and throughflow (S_2) surfaces (see Fig. 1). In the resulting set of equations, one for each surface, body forces naturally appear that represent the variation of pressure in the direction normal to this stream surface. The force acts along the unit normal vector s to the stream surface. Hence we have:

$$F = fs$$

Note that F is orthogonal to the relative velocity of the fluid with respect to a frame of reference fixed on the blades. Thus, we can write:

$$F \cdot u_R = 0$$

with u_R the velocity relative to the blade frame of reference. One can interpret f as the force acting along s that is necessary to maintain a particle of fluid on a given stream surface. Pitch-averaged equations in a blade passage yield similar results.[2] In this case the force is related to the pressure difference between suction and pressure sides of the blade. Moreover, it can be shown that for incompressible flows, under the assumption of an infinite number of blades, the solution of the throughflow equations yields circumferentially averaged values of flow and fluid properties if some measure of the blade loading is small.[9,12]

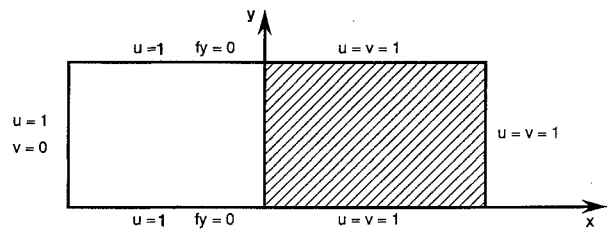

Fig. 2 Analytical solution: two-dimensional case.

These methods have two major restrictions. They are limited to a given flow configuration and are valid for inviscid flows only. The specific equations of Wu depend on the type of flow considered: radial, axial, or mixed. One must decide a priori on the proper set of equations that best fits the flow configuration. However, this is not always possible. For instance, in a Francis turbine the flow is radial in some regions and axial in others. Although separate analyses may be performed for various parts of the flow, a global analysis is complex. Consider, for instance, a rotor-stator combination. For this configuration, two frames of reference must be used, a rotating one for the rotor and a fixed one for the stator, and solutions must be patched from one region to the other. An additional requirement is that the equations must remain valid in the absence of blades (i.e., they must reduce to the usual Navier-Stokes form).

Our extension of Wu's theory and pitch-averaged approximation to viscous flows leads to the following generalization of the equations of motion[13]:

$$\rho D_t(u) = \mathrm{div}(\sigma) + fs \tag{1}$$

$$\mathrm{div}(u) = 0 \tag{2}$$

$$u \cdot s + k = 0 \tag{3}$$

$$k = -v \cdot s \tag{4}$$

where $v = r\omega$ is the blade entrainment velocity vector. Equations (1) and (2) are the usual Navier-Stokes equations, while Eq. (3) states the tangency of the pitch-averaged velocity vector u to the mean stream surface in the bladed region. Equation (3) is valid for all flow configurations (axial, radial, mixed flows) and accounts implicitly for the rotating motion of the blades. Note that blades are assumed infinitely thin; hence blockage effects are included at present. Furthermore, in the absence of blades s equals zero, Eq. (3) is automatically verified, and no force is applied on the fluid; Eqs. (1–3) reduce to the usual Navier-Stokes equations. Thus we have a natural coupling between rotor, stator, and duct regions. It is noted that, at present, pressure losses due to shear on the blades have been neglected. This is not a serious restriction since most profiles are designed with high lift-to-drag ratio.[14] A loss term can be incorporated easily into the model. An appropriate correction term for losses can be incorporated readily into the model.

The present model is best suited for conditions near the propeller design point. For off-design conditions, the throughflow model alone is insufficient, since the lift-to-drag ratio is no longer large because shear losses on the blade surface become important. An approach for improving the prediction of the throughflow code would consist in coupling it with a viscous blade-to-blade analysis program; this results in a viscous quasi-three-dimensional code whose predictions, are valid over a wider range of off-design conditions.

Nature of the Force Term: Two Analytical Solutions

We consider the uniform flow in a section of an infinite domain that is required to follow a sudden change of direction as illustrated in Fig. 2. Because the solution is a function of streamwise distance, only a finite portion of the domain

need be considered. Without loss of generality, we set $\rho = 1$, $\mu = 0.1$, and assume that the flow is at 45 deg on the right of the origin. A simple analysis shows that the analytical solution is given by:

$$u = 1 \quad \text{for all } x$$

$$v = \begin{cases} e^{10x} & \text{for } x < 0 \\ 1 & \text{for } x \geq 1 \end{cases}$$

$$p = \begin{cases} 0 & \text{for } x < 0 \\ -1 & \text{for } x \geq 0 \end{cases}$$

$$f = \begin{cases} 1 & \text{for } x = 0 \\ 0 & \text{for } x \geq 0 \end{cases}$$

In this example, the flow is uniform downstream of $x = 0$. Hence, there should be no force applied in the fluid. A simple balance of forces, on the interface at $x = 0$, indicates that the preceding solution is correct and shows that the blade force in this case is only defined on the leading edge of the cascade and takes the form of a Dirac mass. Note that while the velocity field is continuous, the pressure is discontinuous. The possibility of having discontinuous pressures will significantly affect the choice of pressure approximation in the finite-element model.

Consider now the flow inside an annulus filled with very closely spaced twisted ribbons. For this case the blade normal is given by $s = (s_z, s_r, s_\theta) = (-\sin\alpha, 0, \cos\alpha)$ where α is the angle between the ribbon and the meridional plane. The analytical solution is given by:

$$u_z(r) = Dr^B + Er^{-B} + CAr^2$$

$$u_\theta(r) = \tan(\alpha)(Dr^B + Er^{-B} + CAr^2) + \omega r$$

$$f(r) = -\mu \frac{\tan(\alpha)}{\cos(\alpha)} \left[\frac{B^2 - 1}{r^2} (Dr^B + Ee^{-B}) + 3AC \right]$$

where the coefficients A, B, C, D, and E are functions of the geometry and fluid properties only. In this last problem, the velocity, pressure, and force field are all continuous functions.

Although these two examples represent extreme cases, they illustrate the features that must be embodied in the numerical algorithm if meaningful results are to be obtained.

1) The pressure approximation must allow for discontinuities.

2) The blade-force approximation in the throughflow plane must be constructed of two parts: a body force (f_v) inside region swept by the blade and a Dirac distribution along its boundary (f_s) (see Fig. 3).

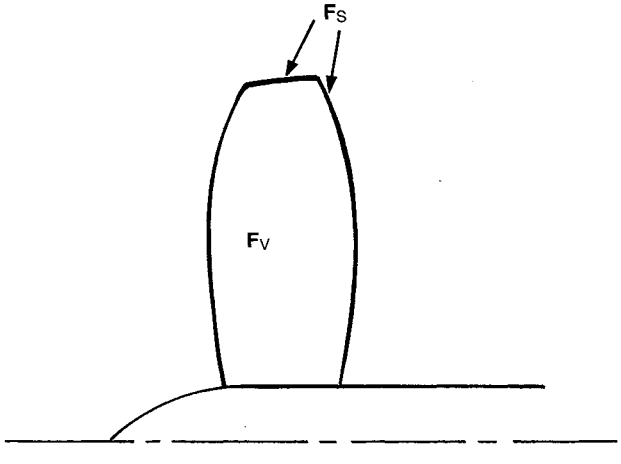

Fig. 3 Blade-force approximation.

Kinematic Modeling of the Propeller

The distribution of s, the mean stream surface, normal vector, is required to close the problem. The blade geometry of the three-bladed rotor tested in Ref. 11 was input to propeller performance codes using lifting line theory and Prandtl tip loss factor,[14,15] thus the effects of bound and free vortices are included. Because the rotor has very few blades, this constitutes a severe test case for our approach.

The programs produce a radial distribution of axial and swirl velocity just behind the rotor. Conversion of these distributions into flow angles determines the values of s at the backface of the propeller. To extend the specification of s inside the propeller region, we assumed that s is constant for a given radius [i.e., $s = s(z)$]. This is a reasonable approximation when the blades of the propeller are very slender. This may cause some error due to thickness effects, most notably near the root sections. Fortunately, the root sections of airplane propellers produce little thrust. Indeed, the bulk of the trust is produced by the outer blade section (60–85% of blade radius).

It is well known that lifting-line theory provides global values of thrust and torque that are sometimes in slight disagreement with propeller performance data. If such data are available, it is possible to improve somewhat the estimate of s by scaling the flow angles from lifting-line theory so that thrust and torque estimates match the data.

Turbulence Model

Following Refs. 7 and 8, turbulence is modeled using Boussinesq's eddy-viscosity concept,[16] which assumes that turbulent stresses are proportional to the mean-velocity gradients. Use has been made of this hypothesis in Eqs. (1–3) so that the effective viscosity may be expressed as

$$\mu = \mu_l + \mu_t \tag{5}$$

where μ_t is the turbulent viscosity that, in contrast to μ_l, the molecular viscosity, is not a fluid property but depends on the state of turbulence; μ_t may vary from point to point in the flow. To close the equations of motion, the eddy viscosity must be related to the other unknowns of the problem. The flow behind a propeller is very similar to jets and wakes. Indeed, a velocity excess is present downstream of the thrusting part of the propeller, and a defect is also present near the root and tip of the blade. See Refs. 7, 8, and 11 for experimental evidence. Hence a mixing length model is used. This is done through the use of the relationship

$$\mu_t = \rho L_m^2 \{[\text{grad}(\boldsymbol{u}) + \text{grad}(\boldsymbol{u})^T] : \text{grad}(\boldsymbol{u})\}^{1/2} \tag{6}$$

where L_m is a characteristic length scale of the shear layer. It now remains to specify the length scale L_m. Following Ref. 16, we adopt the simplest possible form:

$$L_m = 0.09\delta \tag{7}$$

where δ is defined as the distance between points such that the velocity differs from the freestream by 10% of the maximum velocity difference across the layer. For symmetric flows, δ is the distance from the axis of symmetry to the 10% point at the outer edge of the free shear layer. Since the width of the free shear layer will not vary much in the near field of the propeller wake, we take $\delta = 90\%$ of the propeller radius. More sophisticated models with variable L_m, or using the integrated TKE[7] equation can be implemented readily in the current code. The current mixing length model is closely related to the more sophisticated integrated TKE model of Refs. 7 and 8 that has proved to be reliable for the class of flows of interest.

It should be noted that Eq. (6) is defined in terms of an invariant of the flowfield. Hence, μ_t is independent of the coordinate system used for the simulation, and important

property that is sometimes overlooked. When substituted in Eq. (1), this formula introduces strong nonlinearities in the equations of motion.

Solution Algorithm

Penalty Function Formulation

A standard Bubnov-Galerkin formulation is used,[17,18] hence the interpolation functions and test functions are identical. Details of the weak Galerkin formulation of Eqs. (1–3) are readily available for penalty formulation.[18] Thus, only an outline of the technique is presented here. It is well known that the velocity lies in $H_0^1(\Omega)$ and the pressure in $L^2(\Omega)$,[19] but the space containing the force is more complex; it is the dual of the velocity space, thus:

$$f \in [H^1(\boldsymbol{D})]' = H^{-1}(\boldsymbol{D}) \oplus H^{-1/2}(\partial \boldsymbol{D}) \tag{8}$$

This decomposition results from the requirement that the tangency condition be satisfied within the bladed region and on its boundary. A similar behavior was noted for the two analytical solutions of the previous section. Unfortunately, $H^{-1}(\boldsymbol{D})$ and $H^{-1/2}(\partial \boldsymbol{D})$ are highly irregular spaces, and to develop a computational model, one must assume more regularity. This is achieved by using the following decomposition:

$$f = f_v + f_s \delta_s \tag{9}$$

and by assuming that

$$f_v \in L^2(\boldsymbol{D}) \subset H^{-1}(\boldsymbol{D})$$

$$f_s \in L^2(\partial \boldsymbol{D}) \subset H^{-1/2}(\partial \boldsymbol{D})$$

where δ_s is the Dirac function defined on $\delta \boldsymbol{D}$. Although the decomposition of Eq. (9) implies more regularity on f than Eq. (8), it still provides enough flexibility for our purpose.

Substitution of an approximate solution (u^*, p^*, f^*) into Eqs. (1–3) yields a set of residual equations of the form

Momentum:

$$f_1(\boldsymbol{u}^*, p^*, f^*) = \boldsymbol{R}_1$$

Continuity:

$$f_2(\boldsymbol{u}^*) = \boldsymbol{R}_2$$

Tangency:

$$f_3(\boldsymbol{u}^*) = \boldsymbol{R}_3$$

where $\boldsymbol{R}_i$ are the residuals, a measure of the quality of the approximate solution. The Galerkin method reduces this error to zero by making it orthogonal to a certain set of functions. The continuity and tangency equation constraints are enforced by using a consistent penalty method to assure that proper weak forms are obtained.[19,20] The resulting weak formulation is given by

$$\int_\Omega \rho D_t(\boldsymbol{u}) \cdot \delta \boldsymbol{u}\, d\Omega + \int_\Omega \mu \tau : \operatorname{grad}(\delta \boldsymbol{u})\, d\Omega + \int_\Omega \lambda \operatorname{div}(\boldsymbol{u}) \operatorname{div}(\delta \boldsymbol{u})\, d\Omega + \int_D \beta(\boldsymbol{u} \cdot \boldsymbol{s} + k)\boldsymbol{s} \cdot \delta \boldsymbol{u}\, d\Omega + \int_{\partial D} \beta(\boldsymbol{u} \cdot \boldsymbol{s} + k)\boldsymbol{s} \cdot \delta \boldsymbol{u}\, d\Gamma = \int_{\partial \Omega} t_s \cdot \delta \boldsymbol{u}\, d\Gamma \tag{10}$$

Here β and λ are positive numbers whose values affect the accuracy of the solution, while $\delta \boldsymbol{u}$ may be interpreted as a virtual velocity. Equation (10) is then similar to the principle of virtual work of solid mechanics.

The divergence theorem was applied to the stress tensor σ to reduce the differentiability requirement on the velocity by transferring some of the derivatives from $\boldsymbol{u}$ to $\delta \boldsymbol{u}$ and to introduce the natural boundary conditions involving the surface tractions t_s:

$$t_s = \sigma \cdot \boldsymbol{n} \tag{11}$$

The pressure does not appear explicitly in Eq. (10); it appears only implicitly through the surface integrals on the right-hand side of Eq. (10). The only unknowns are the velocity components. This results in significant computational savings. Once the velocity field is obtained by solving Eq. (10); pressure and forces are recovered in a postprocessing step[13] through

$$p = -\lambda \operatorname{div}(\boldsymbol{u})$$

$$f_v = -\beta(\boldsymbol{u} \cdot \boldsymbol{s} + k) \text{ in the bladed region}$$

$$f_s = -\beta(\boldsymbol{u} \cdot \boldsymbol{s} + k) \text{ on the edge of the bladed region} \tag{12}$$

Convergence of the solution of the penalty formulation to the true solution, as $\lambda \to \infty$ and $\beta \to \infty$, can be proved.[17,18] Values of 10^6–10^8 usually prove effective.[7,8]

Choice of Element Interpolation

There remains to construct a finite-element approximation to Eq. (10). The biquadratic velocity with discontinuous linear pressure element has proven to be one of the most successful approximations for incompressible flow simulations and is used outside the blade. A discontinuous pressure approximation must be used since it was shown that the pressure field may have discontinuities.

The proper choice of approximation for f is a more complicated matter. A careful study of analytical solutions[7,13] reveals that the tangency condition is a very severe constraint on the flowfield. In fact, for planar cases the form of "$\boldsymbol{s}$" completely determines the streamlines and hence the solution. For swirling flows, there are three velocity components, and Eq. (3) only specifies part of the flowfield. It was found that a piecewise constant approximation was adequate in the volume swept-by blade, but that a quadratic approximation was needed on its boundary. This seemingly unusual combination can be partially explained by the fact that proper satisfaction of Eq. (3) on the edge is crucial to the solution, and hence more degrees of freedom are needed for the surface force f_s.

General Solution Procedure

From a practical point of view, the elements are treated in three groups: regular Navier-Stokes flow elements, "rotor/stator" elements incorporating the volume force terms within the blade region, and edge elements with surface forces. The element equations are assembled in a compacted skyline storage format. The formulation results in a system of nonlinear algebraic equations of the form

$$K(\boldsymbol{U})\boldsymbol{U} = \boldsymbol{F} \tag{13}$$

where K is the global system matrix, $\boldsymbol{U}$ the global vector of unknowns, and $\boldsymbol{F}$ the global vector resulting from the boundary conditions and the rotation of the blades.

This system of equations may be solved by a combination of iterative methods: successive substitution and Newton-Raphson. If needed, the eddy viscosity is updated at each iteration using the current velocity distribution. The linearized system of equations is very large and is solved by direct Gaussian decomposition.

Although the quadratic convergence of Newton's method makes it a powerful solution procedure, it is somewhat limited in terms of its radius of convergence. An appealing technique to overcome this shortcoming is first to use the successive substitution method that has a wider radius of convergence but a somewhat slower convergence rate. The following strategy was found suitable throughout this study: starting from

an initial guess of the velocity field (zero velocity), perform 2 or 3 steps of successive substitution, then switch to Newton-Raphson and iterate until convergence. Both iteration schemes can be cast in a standard format:

$$[K(u^n) + J(u^n)]\,\Delta U = -R(U^n)$$

$$U^{n+1} = U^n + \alpha \Delta U$$

The matrix J contains the terms arising from the Newton linearization ($J = 0$ for successive substitution), and R is the residual from Eq. (13)

$$R(U^n) = F - K(U^n)U^n$$

The parameter α controls the degree of relaxation.

Results and Discussion

The propeller and turbulence model were programmed and interfaced to the author's general purpose finite-element fluid dynamics program CADYF. The resulting code can simulate planar, axisymmetric, turbulent free shear flows. Calculations were performed on a sequence of successively refined grid until grid independent solutions were obtained. Typical computing times are of the order of 2 to 3 min on an IBM 3090-VF.

Nondimensionalization

All calculations were performed with a nondimensional form of the equations of motion for the conditions of Ref. 11. Reference values are selected for the velocity U_0^*, length L_0^*, and pressure P_0^* to obtain the following dimensionless variables (the asterisk denotes a dimensional variable):

$$x_i = \frac{x_i^*}{L_0^*}, \quad u_i = \frac{u_i^*}{U_0^*}, \quad p = \frac{p^* - P_0^*}{\rho^* U_0^{*2}}$$

$$f_v = \frac{f_v^*}{\rho^* U_0^{*2}/L^*}, \quad f_s = \frac{f^*}{\rho^* U_0^{*2}}$$

$$\mu = \frac{\mu^*}{\rho^* U_0^* L_0^*} = \frac{1}{\mathrm{Re}_\mu}, \quad \rho = \frac{\rho^*}{\rho_0^*} = 1$$

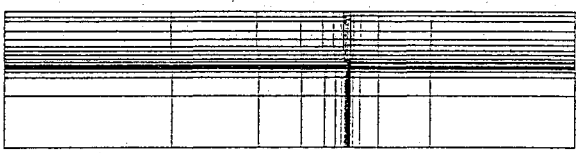

Fig. 4 Grid for propeller flow.

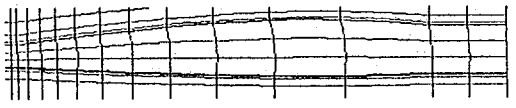

Fig. 5 Detail of grid near the propeller.

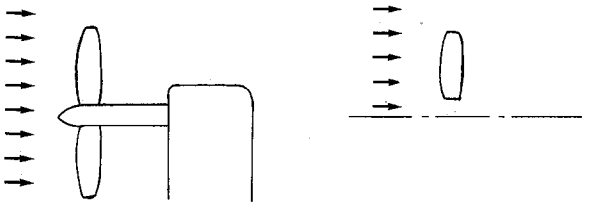

Fig. 6 Experimental and numerical configurations.

Uniform Flow Past a Propeller

The characteristics of the flow are $U_0^* = 8.52$ m/s, $L_0^* = 0.492$ m, $N = 1150$ rpm, $\rho_0^* = 1.179$ kg/m^3, and $\mu_l^* = 1.8 \times 10^{-5}$ kg/(s · m). The grid is a rectangle with 47 nodes in the axial direction and 37 in the radial direction (Figs. 4 and 5). The inflow boundary is located two diameters upstream of the propeller. While the outflow plane stands at three diameters downstream of the propeller, the freestream boundary is a cylindrical shell of radius 1.2 diameters. At the inflow, u_x is set to unity, and u_r and u_θ are set to zero. On the freestream boundary, u_x is set to one, and the r and θ tractions, Eq. (11), are set to zero. The three components of the traction vector are set to zero at the outflow boundary.

The mean flow quantities are not all predicted or measured with the same accuracy. For the present finite-element scheme, the three velocity components are the most accurately predicted, while the pressure prediction is less accurate. For the experiments of Kotb,[11] the order of decreasing accuracy in the measurements of the mean flow properties is axial velocity, pressure, swirl, and, lastly, radial velocity. It should be noted that the analysis does not include the shaft and drive-train housing of the experiments (Fig. 6). A body is placed close to and downstream of the propeller to house the drive train. The housing begins at 0.23 propeller diameter downstream of the disk. The presence of the housing probably will affect the experimental results from the station located at $x/D = 0.23$ since this station sits right on the body. The shaft could be included in the current analysis; however, extensive changes to the turbulence model would be necessary to include the no-slip condition on the shaft. Inclusion of the body would require a fully three-dimensional simulation that is clearly beyond the scope of this paper.

Figure 7 compares the experimental and predicted axial velocity profiles. The agreement is excellent at $x/D = 0.025$, while at $x/D = 0.23$ the experimental velocity distribution is higher than the numerical prediction. This is probably due to the presence of the drive housing that acts as an obstacle and decreases the wind tunnel cross section, thus increasing the measured velocity.

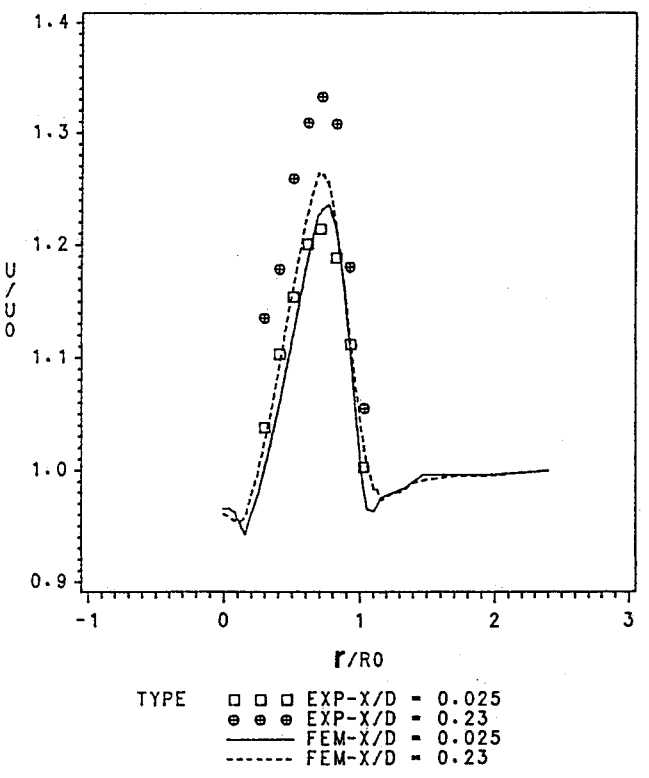

Fig. 7 Axial velocity profile.

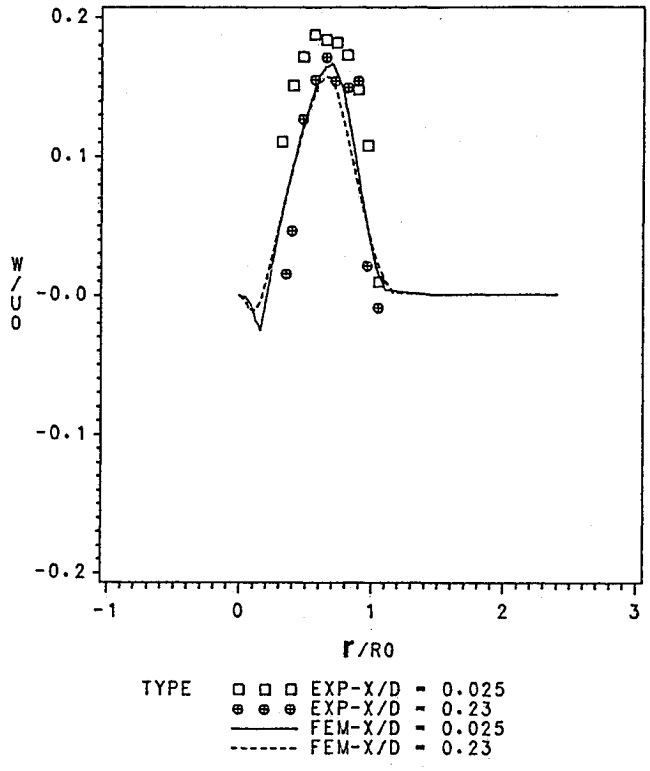

Fig. 8 Swirl profile.

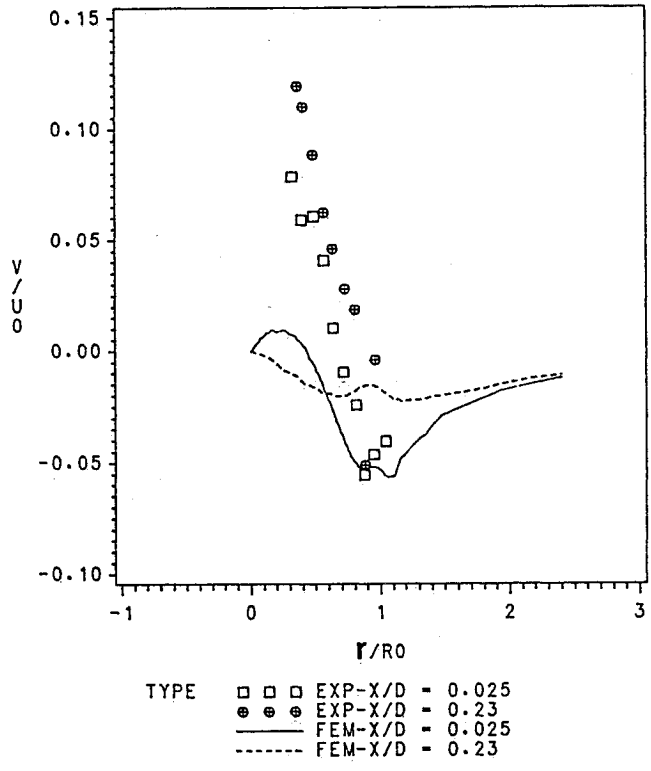

Fig. 9 Radial velocity profile.

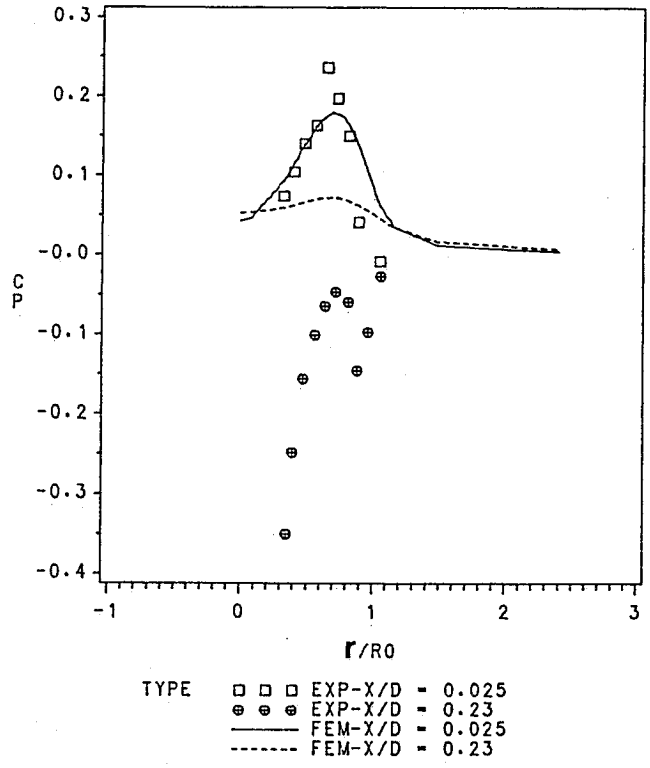

Fig. 10 Pressure distribution.

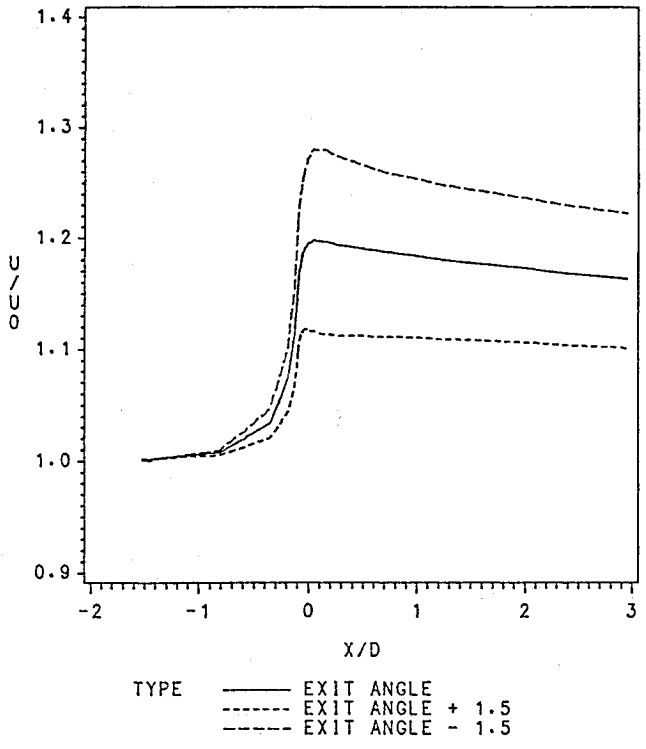

Fig. 11 Streamwise distribution of axial velocity.

Figure 8 presents the predicted and experimental swirl profiles. Agreement between prediction and experiments is excellent. The overall quality of the swirl prediction should be viewed as very good and constitutes a major improvement over those of Ref. 21 and confirms the results of Ref. 7 obtained with a body force model for the propeller.

Figure 9 compares the predicted and measured radial velocity distributions. The prediction curves display the expected shape for a free-running propeller: outward flow close to the axis and inward contraction farther out in the freestream, both due to acceleration of the fluid. This component of the velocity is the most difficult to measure and is subject to the highest experimental uncertainty. At the first station ($x/D = 0.025$), the experiments display a behavior similar to that of the predictions, but the magnitudes do not agree. At the second station ($x/D = 0.23$), the experimental velocity distribution is directed outward, while that of the predictions

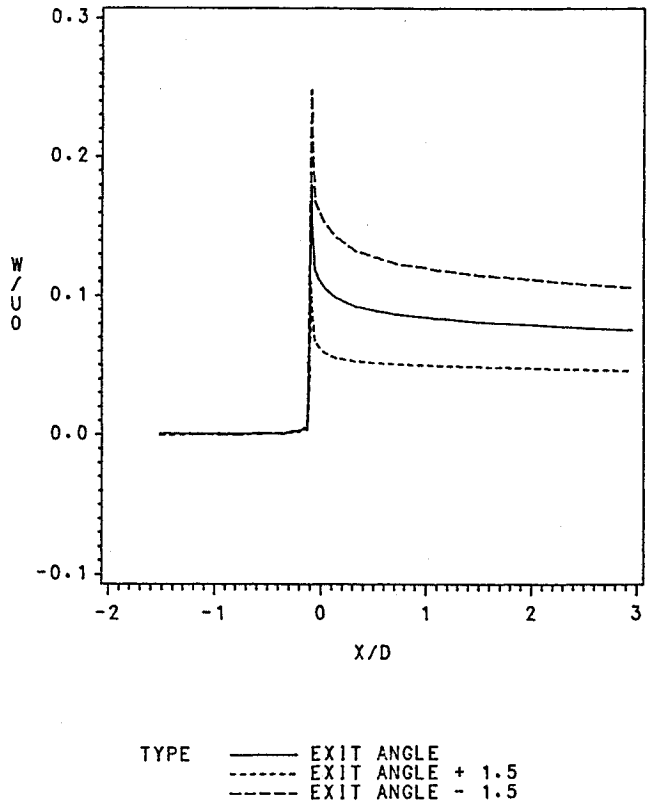

Fig. 12 Streamwise distribution of swirl.

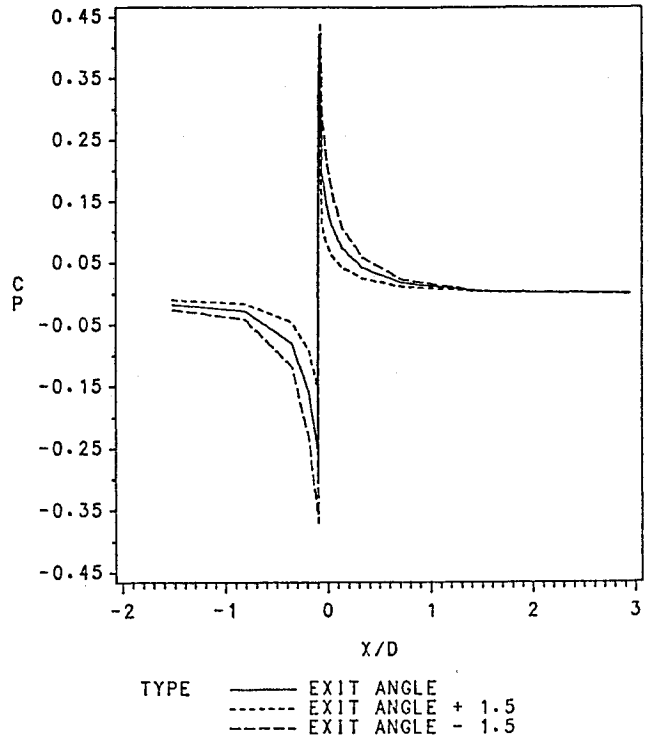

Fig. 13 Streamwise distribution of pressure.

points mostly inward. This experimental behavior probably is due to the presence of the drive housing.

Figure 10 presents the predicted and experimental radial profiles of pressure. The pressure is given in the form of a pressure coefficient, $C_p = 2(p^* - P_0^*)/(\rho^* U_0^{*2})$, with $P_0^* = 0$ the freestream pressure. Given the lower accuracy expected on the pressure prediction, the agreement with the experiments is good at the first station ($x/D = 0.025$). The pressure predicted at the second station is in qualitative agreement with the theory of free-running propellers. One clearly sees the relaxation of the pressure toward its freestream value. The experimental profiles at the second station ($x/D = 0.23$) have negative values typical of the flow over an obstacle such as the drive housing.

Figures 11–13 present calculated streamwise distribution of axial and swirl components and pressure, respectively. These distributions were extracted at 85% of the propeller radius. In the current analysis, the radial distribution of the flow angle at the propeller outlet was given by a performance code. Based upon this distribution, a field "s" then was constructed and input into the "kinematic" relationship of the propeller model [Eq. (3)]. One clearly sees the extreme sensitivity of the flow to small variation in the radial distribution of the propeller exit angle (± 1.5 deg).

Concluding Remarks

A new model has been developed to simulate the flow past propellers. The technique includes the effect of the blades on the flow without necessitating the solution of fully three-dimensional time-dependent flows. The main results can be summarized as follows:

1) Predictions for uniform flow past a propeller show excellent agreement with the experiments for axial and swirl component of the velocity and good agreement for the pressure.

2) Numerical simulations show that the velocity and pressure fields are very sensitive to the "kinematic" modeling of the propeller.

3) Previous work required knowledge of the dynamics of the propeller thrust and torque. In this analysis the propeller is modeled by a simple kinematic relationship for the tangency equation.

4) The resulting Galerkin finite-element algorithm is robust and stable, mostly due to the full coupling of the three momentum equations, the continuity equation, and the tangency equation.

Future plans and extensions of the analysis involve including thickness effect through the blockage factor B. The sensitivity of the predictions to the blade exit angle could be eliminated by coupling the present throughflow analysis to a blade-to-blade code making it possible to perform viscous quasi-three-dimensional simulations. This would eliminate the reliance on a propeller performance code to determine the mean stream surface. This more elaborate model also would provide detailed information on local blade loading and propeller performance.

Acknowledgments

This work was supported in part by the Natural Sciences and Engineering Research Council of Canada, the Centre de Recherche Informatique de Montréal, and the Office of Naval Research, through cooperative research with J. A. Schetz of the Aerospace and Ocean Engineering Department, Virginia Polytechnic Institute and State University, Blacksburg, Virginia. Finally, constructive comments by the reviewers are gratefully acknowledged.

References

[1]Vu, T. C., Shyy, W., Braaten, M. E., and Reggio, M., "Recent Developments in Viscous Flow Analysis for Hydraulic Turbine Components," International Association for Hydraulic Research Symposium, Sept. 1986, Montreal, Canada.

[2]Adamczyk, J. J., and Graham, R. W., "Numerical Simulation of Multiblade Row Turbomachinery Flows," *CRAY Channels*, Summer 1986.

[3]Strouboulis, T., Devloo, P., and Oden J. T., "A Moving-Grid Finite Element Algorithm for Supersonic Flow Interaction Between Moving Bodies," *Computational Methods in Applied Mechanics and*

Engineering, Vol. 59, 1986, pp. 235–255.

[4]Von Kármán, T., and Burgers, J. M., "General Aerodynamic Theory-Perfect Fluids," *Aerodynamic Theory*, Vol. 2, edited by W. F. Durand, California Institute of Technology, Pasadena, CA, 1964.

[5]Sparenberg, J. A., "On the Potential Theory of the Interaction of an Actuator Disk and A Body," *Journal of Ship Research*, Vol. 16, Dec. 1972, pp. 271–277.

[6]Sparenberg, J. A., "On the Linear Theory of an Actuator Disk in a Viscous Flow," *Journal of Ship Research*, Vol. 18, No. 1, March 1974, pp. 16–21.

[7]Pelletier, D., and Schetz, J. A., "Finite Element Navier-Stokes Calculation of Three-Dimensional Flow Near a Propeller," *AIAA Journal*, Vol. 24, No. 9, 1986, pp. 1406–1409.

[8]Schetz, J. A., Pelletier, D., and Mallory, D., "Numerical and Experimental Investigation of a Propeller Flowfield with a 3-D Non-Uniform Inflow," AIAA Paper 87-0607, Jan. 1987.

[9]Horlock, J. H., *Actuator Disk Theory*, McGraw-Hill, New York, 1978.

[10]Wu, C. H., "A General Theory of Three-Dimensional Flow in Subsonic and Supersonic Turbomachines of Axial Radial, and Mixed-Flow Types," NASA TN-2604, Jan. 1952.

[11]Kotb, M. A., "Experimental Investigation of 3-D Turbulent Free Shear Flows Past Propellers and Windmills," Ph.D. Dissertation, Aerospace and Ocean Engineering Dept., Virginia Polytechnic Institute and State University, Blacksburg, VA, Oct. 1984.

[12]Ruden, P., "Investigation of Single Stage Axial Fans," NACA TM 1062, 1944.

[13]Garon, A., "Modèle pour l'étude des écoulements visqueux et incompressibles dans les turbines hydrauliques," Ph.D. Dissertation, Ecole Polytechnique de Montréal, Montreal, Canada, May 1987.

[14]Durand, W. F., "Aerodynamic Theory," *Division-L-Airplane Propellers*, edited by H. Glauert, Dover, New York, 1963, Chap. 1.

[15]Schwartz, L. W., and Bernstein, S., "Documentation of a Propeller Analysis Computer Program," Flow Research, Washington, DC, Flow Research No. 67, March 1975.

[16]Rodi, W., *Turbulence Models and Their Application in Hydraulics*, International Association for Hydraulic Research, Rotterdam, the Netherlands, June 1980.

[17]Reddy, J. N., *Applied Functional Analysis and Variational Methods in Engineering*, McGraw-Hill, New York, 1986.

[18]Carey, G. F., and Oden, T. J., *Finite Elements: A Second Course*, Prentice-Hall, Englewood Cliffs, NJ, 1983.

[19]Pelletier, D., Garon, A., and Camarero, R., "A Finite Element Method for Computing the Flow Inside Rotating Machinery," Eighth International Conference on Computing Methods in Applied Sciences and Engineering, Versailles, France, Dec. 14–18, 1987.

[20]Engelman, M. S., Sani, R. L., Gresho, P. M., and Bercovier, M., "Consistent vs. Reduced Quadrature Penalty Methods for Incompressible Media Using Several Old and New Elements," *International Journal of Numerical Methods for Fluids*, Vol. 2, No. 1, 1982.

[21]Schetz, J. A., and Favin B., "Numerical Solution of a Body-Propeller Combination Flow Including Swirl and Comparison with Data," *Journal of Hydraunautics*, Vol. 13, No. 2, April 1979, pp. 46–51.